



Title	Green-Kubo measurement of liquid-solid friction in finite-size systems
Author(s)	Oga, Haruki; Yamaguchi, Yasutaka; Omori, Takeshi et al.
Citation	Journal of Chemical Physics. 2019, 151(5), p. 054502-1-054502-9
Version Type	VoR
URL	https://hdl.handle.net/11094/83322
rights	© 2019 Author(s). This article is licensed under a Creative Commons Attribution 4.0 International License.
Note	

The University of Osaka Institutional Knowledge Archive : OUKA





<https://ir.library.osaka-u.ac.jp/>

The University of Osaka

Green-Kubo measurement of liquid-solid friction in finite-size systems

Cite as: J. Chem. Phys. **151**, 054502 (2019); <https://doi.org/10.1063/1.5104335>

Submitted: 26 April 2019 . Accepted: 07 July 2019 . Published Online: 05 August 2019

Haruki Oga , Yasutaka Yamaguchi , Takeshi Omori , Samy Merabia , and Laurent Joly 



View Online



Export Citation



CrossMark

The Journal
of Chemical Physics

Submit Today

The Emerging Investigators Special Collection and Awards
Recognizing the excellent work of early career researchers!

Green-Kubo measurement of liquid-solid friction in finite-size systems

Cite as: J. Chem. Phys. 151, 054502 (2019); doi: 10.1063/1.5104335

Submitted: 26 April 2019 • Accepted: 7 July 2019 •

Published Online: 1 August 2019



Haruki Oga,^{1,a)} Yasutaka Yamaguchi,^{1,2,b)} Takeshi Omori,^{1,c)} Samy Merabia,³ and Laurent Joly³

AFFILIATIONS

¹Department of Mechanical Engineering, Osaka University, 2-1 Yamadaoka, Suita 565-0871, Japan

²Water Frontier Science and Technology Research Center (W-FST), Research Institute for Science and Technology, Tokyo University of Science, 1-3 Kagurazaka, Shinjuku-ku, Tokyo, 162-8601, Japan

³Univ Lyon, Univ Claude Bernard Lyon 1, CNRS, Institut Lumière Matière, F-69622 Villeurbanne, France

^{a)}Electronic mail: haruki@gcom.mech.eng.osaka-u.ac.jp

^{b)}Electronic mail: yamaguchi@mech.eng.osaka-u.ac.jp. URL: <http://www-gcom.mech.eng.osaka-u.ac.jp/>.

^{c)}Electronic mail: tomori@mech.eng.osaka-u.ac.jp

ABSTRACT

To characterize liquid-solid friction using molecular dynamics simulations, Bocquet and Barrat (BB) [Phys. Rev. E **49**, 3079–3092 (1994)] proposed to use the plateau value of a Green-Kubo (GK) integral of the friction force. The BB method is delicate to apply in finite-size simulations, where the GK integral vanishes at long times. Here, we derive an expression for the GK integral in finite-size systems, based on a Langevin description of a coarse-grained system effectively involving a certain thickness of liquid close to the wall. Fitting this expression to GK integrals obtained from simulations of a liquid slab provides the friction coefficient and the effective thickness of the coarse-grained system. We show that the coarse-grained system for a Lennard-Jones fluid between flat and smooth solid surfaces is 2–3 molecules thick, which provides a criterion for measuring the friction coefficient independently of confinement. As compared to nonequilibrium simulations, the new approach is more accurate and removes some ambiguities of nonequilibrium measurements. Overall, we hope that this new method can be used to characterize efficiently liquid-solid friction in a variety of systems of interest, e.g., for nanofluidic applications.

© 2019 Author(s). All article content, except where otherwise noted, is licensed under a Creative Commons Attribution (CC BY) license (<http://creativecommons.org/licenses/by/4.0/>). <https://doi.org/10.1063/1.5104335>

I. INTRODUCTION

To describe flows in macroscopic channels, one can combine a continuum description of mass transport in the bulk (e.g., the Navier-Stokes equation) with a no-slip boundary condition (BC) for the fluid velocity at the wall. Such a macroscopic description is expected to fail to capture flows in nanofluidic systems,^{1,2} which offer great promises of application in green energies^{3–5} and water treatment.^{6–8} Yet, it has been discussed that for water the continuum description of the bulk flow should remain valid down to typically 1 nm.¹ In contrast, both experiments and molecular simulations have shown that the no-slip BC can fail when liquid-solid friction is low enough.^{9,10}

In the presence of slip, the hydrodynamic BC is obtained by writing that the viscous shear stress in the liquid at the wall, $\eta\partial_z v$

(with η being the shear viscosity, z being the direction normal to the interface, and v being the velocity parallel to the interface), is equal to the interfacial friction shear force per area τ_w , proportional to the slip velocity v_s (the jump of parallel velocity at the interface), as initially discussed by Navier,^{11,12}

$$\tau_w = \lambda v_s. \quad (1)$$

Equation (1) defines the (fluid) friction coefficient λ , a critical parameter controlling flows in nanofluidic systems.

Molecular dynamics (MD) simulations, which explicitly describe the atomistic details of liquid-solid interfaces, can be instrumental in measuring the friction coefficient^{13–25} and in exploring the underlying mechanisms.^{26–35} Friction can be measured directly in nonequilibrium MD (NEMD) simulations of a flowing liquid.

However, the direct approach is time consuming and poses different issues^{20,36–38} related to, e.g., the choice of the thermostatting method, the necessary tests on the linear response of the system, or the definition of the effective position of the hydrodynamic boundary. Alternative approaches have been proposed based on equilibrium molecular dynamics (EMD). In particular, Bocquet and Barrat (BB) introduced a Green-Kubo (GK) expression where the friction coefficient is obtained as the plateau value at long times of a GK integral,¹³

$$\lambda = \lim_{t \rightarrow \infty} \Lambda(t), \text{ with } \Lambda(t) = \frac{1}{Sk_B T} \int_0^t \langle F_w(0)F_w(t') \rangle dt, \quad (2)$$

where S , k_B , T , and F_w denote the surface area, Boltzmann constant, absolute temperature, and instantaneous shear force exerted on the solid, respectively, and the angular brackets $\langle \rangle$ mean the ensemble average.

However, applying the BB formula in MD simulations poses a number of issues.^{17,21–23} In particular, simulations are limited to finite-size systems, where it has been discussed that GK integrals should vanish at infinite time instead of reaching a plateau corresponding to the response coefficient,^{39,40} an issue sometimes referred to as “the plateau problem.”^{41,42} Different solutions have been suggested to the plateau problem. For instance, the maximum of the GK integral—or the value of the GK integral at the first zero of the autocorrelation function—has been used to estimate the friction coefficient.^{13,43–47} Alternative equilibrium^{18–20,22,23,25,42} and nonequilibrium^{14,15} methods have been developed. Recently, Español, de la Torre, and Duque-Zumajo⁴¹ have proposed a general solution to the plateau problem within the context of Mori projection operator formulation, which could in principle be applied to the GK measurement of the liquid-solid friction coefficient. The fundamental statistical physics underlying the BB formula has also been discussed in two recent theoretical articles.^{48,49} Nakano and Sasa⁴⁸ started from the Hamiltonian of the particle system and, by considering the local detailed balance condition, examined the applicability of existing expressions of the liquid-solid friction from a viewpoint of time- and length-scale separation, which can be evaluated from hydrodynamics behavior. On the other hand, Camargo *et al.*⁴⁹ considered the mechanical balance and local constitutive equation of a thin slab of layered fluid formed near the wall covering the liquid-solid interface (mentioned as a “pillbox” for a spherical interface) and derived the boundary condition. In contrast with these recent articles, here we propose a pragmatic approach to extend the BB formula to finite-size systems by introducing a simple expression for the memory kernel and fitting the full GK curve based on a coarse-grained description without dealing with the details of local mechanics. Based on this approach, we show the following two features: (1) an effective mass or thickness of liquid involved in the Langevin equation is obtained as a result and (2) the simple approach of taking the maximum of the GK integral leads to accurate measurements when the memory kernel time scale and the relaxation time scale as a function of the friction coefficient and effective mass are well separated. The two features could consequently correspond to the time- and length-scale separation mentioned in Nakano and Sasa,⁴⁸ and the effective coarse-grained system could also be related to the thin slab in Camargo *et al.*⁴⁹

II. THEORY

The BB formula can be derived based on a generalized Langevin equation (GLE),

$$M \frac{dU}{dt} = -\lambda S \int_{-\infty}^t \xi(t-t') U(t') dt' + R(t), \quad (3)$$

where M and U are the mass and velocity (relative to the wall) of a coarse-grained system of interest, and S , ξ , and $R(t)$ denote the surface area, memory kernel, and random force, respectively. In their analytical derivation, Bocquet and Barrat²¹ described the Brownian motion of a finite-mass wall in contact with a semi-infinite liquid, and M and U were the mass and velocity of the wall, respectively. In MD simulations, however, a liquid confined between two parallel immobile walls is usually considered. In that case, the coarse-grained system should effectively describe the hydrodynamic fluctuations of the liquid. We anticipate that the coarse-grained system can be described as an effective thin region of liquid close to the interface. However, we emphasize that the coarse-grained system encompasses the whole liquid dynamics and that the effective representation by a thin slab of fluctuating liquid should not be taken literally. In particular, viscous friction in the whole liquid is described implicitly through the coarse-graining process and we did not describe it explicitly in the following GLE description; this approach will be validated *a posteriori* by the simulations. We also emphasize that our model differs from previous work^{18,19} where the equation of motion was applied to a liquid slab near the solid because we do not impose any constraint on the mass M of the coarse-grained system, which will be measured from the GK integral.

A full expression for the GK integral can be derived from the GLE, Eq. (3), through the Laplace transform. The complete derivation can be found in the Appendix, and here we only summarize the key steps. Let the Laplace transform of a function $f(t)$ be denoted by $\mathcal{L}(f) \equiv \tilde{f}(s)$. The Laplace transform $\tilde{C}_U(s)$ of the equilibrium autocorrelation function $C_U(t)$ of the velocity U writes

$$\tilde{C}_U(s) = \frac{k_B T}{M} \frac{1}{s + t_d^{-1} \tilde{\xi}(s)}. \quad (4)$$

On the other hand, the force $F_w(t)$ exerted on the coarse-grained system of interest is given by

$$F_w(t) = M \frac{dU}{dt}. \quad (5)$$

Then, the autocorrelation function $C_F(t)$ of the force F_w satisfies the following relation:⁵⁰

$$C_F(t) = -M^2 \frac{d^2 C_U(t)}{dt^2}. \quad (6)$$

Accordingly, the GK integral $\Lambda(t)$ in Eq. (2) writes

$$\Lambda(t) \equiv \frac{1}{Sk_B T} \int_0^t C_F(t') dt' = -\frac{M^2}{Sk_B T} \frac{dC_U(t)}{dt}, \quad (7)$$

where $\left. \frac{dC_U(t)}{dt} \right|_{t=0} = 0$ considering that $C_U(t)$ is an even function due to the stationarity condition.^{51–54} Note that

$$\left. \frac{dC_U(t)}{dt} \right|_{t=0} \equiv \frac{1}{2} \left(\left. \frac{dC_U(t)}{dt} \right|_{t=0^+} + \left. \frac{dC_U(t)}{dt} \right|_{t=0^-} \right) = 0 \quad (8)$$

should be applied in the case the memory kernel $\xi(t)$ is equal to the Dirac delta function, i.e., Eq. (3) is a simple Langevin equation, where $\frac{dC_U(t)}{dt}$ has a discontinuous derivative at $t = 0$, see Refs. 21 and 54. The Laplace transform of Eq. (7) is

$$\tilde{\Lambda}(s) = -\frac{M^2}{Sk_B T} (s\tilde{C}_U(s) - C_U(0)). \quad (9)$$

Inserting Eq. (4) into Eq. (9), it follows that

$$\tilde{\Lambda}(s) = \frac{M}{S} \frac{t_d^{-1} \tilde{\xi}(s)}{s + t_d^{-1} \tilde{\xi}(s)} = \frac{\lambda \tilde{\xi}(s)}{s + t_d^{-1} \tilde{\xi}(s)}. \quad (10)$$

We now assume a simple Maxwell-type memory kernel⁵⁰

$$\xi(t) = t_m^{-1} e^{-\frac{t}{t_m}} \quad (t \geq 0). \quad (11)$$

This memory kernel is originally designed to describe a viscoelastic response; here, we choose it for its simple functional form, although simulations will later show that t_m is indeed compatible with viscoelastic relaxation. We also introduce the characteristic decay time of the GLE

$$t_d \equiv \frac{M}{\lambda S}. \quad (12)$$

Note that through the coarse-graining process, hydrodynamic relaxation in the liquid—controlled by the kinematic viscosity ν —is enclosed implicitly in the coarse-grained mass M/S , and the decay time only depends explicitly on the liquid-solid friction coefficient.

Inserting the Laplace-transformed memory kernel in Eq. (10) and going back to the time domain, one can show that when $t_d > 4t_m$, the GK integral $\Lambda(t)$ in Eq. (2) is given by

$$\Lambda(t) = \lambda_0 \left(e^{-\frac{t}{t_1}} - e^{-\frac{t}{t_2}} \right), \quad (13)$$

where the 3 parameters λ_0 , t_1 , and t_2 can be obtained through

$$\frac{1}{t_1} = \frac{1}{2t_m} \left(1 - \sqrt{1 - \frac{4t_m}{t_d}} \right), \quad (14)$$

$$\frac{1}{t_2} = \frac{1}{2t_m} \left(1 + \sqrt{1 - \frac{4t_m}{t_d}} \right), \quad (15)$$

$$\lambda_0 = \frac{\lambda}{\sqrt{1 - \frac{4t_m}{t_d}}}. \quad (16)$$

Equations (13)–(16) provide a generic framework that can be used to extract the friction coefficient from a fitting of the GK integral. In particular, the friction coefficient can be obtained from the three fitting parameters,

$$\lambda = \lambda_0 \frac{1 - u}{1 + u}, \quad (17)$$

with $u = t_2/t_1$. One can also relate the maximum of the GK integral to λ and to the two time scales of the fit,

$$\Lambda_{\max} = \lambda \frac{1 + u}{1 - u} \left[u^{\frac{u}{1-u}} - u^{\frac{1}{1-u}} \right]. \quad (18)$$

From Eq. (18), it is clear that the maximum of the GK integral Λ_{\max} is not in principle equal to the friction coefficient λ and that Λ_{\max} and λ cannot be related without the knowledge of the characteristic times t_2 and t_1 , which can only be obtained through a full fit of the GK curve. However, when the time scales are well separated, i.e., in the limit of $u \rightarrow 0$, Λ_{\max} becomes an increasingly good estimate of λ : the difference between Λ_{\max} and λ is on the order of 25% for $u = 1/5$ and falls, e.g., to 4% for $u = 1/100$ or to less than 1% for $u = 1/1000$. Note that in the limit where the time scales are separated, the two time scales t_1 and t_2 are given by $t_1 \simeq t_d$ and $t_2 \simeq t_m$, respectively.

Finally, in the limit of $t_d \rightarrow \infty$,

$$\Lambda(t) = \lambda \left(1 - e^{-\frac{t}{t_m}} \right), \quad (19)$$

so that the GK integral reaches a plateau equal to the friction coefficient, which corresponds to the original BB result.

In the following, we will test the general method presented here when the time scales of the memory kernel and of the GK integral decay are not well separated, using MD simulations.

III. SIMULATIONS

We considered a generic Lennard-Jones (LJ) liquid confined between parallel walls, see Fig. 1. We used fcc walls made of 8 atomic layers exposing a (001) face to the liquid; first neighbors in the solids were bound by a harmonic potential $\Phi_h(r) = k/2 (r - r_{eq})^2$, with r being the interparticle distance, $r_{eq} = 0.277$ nm, and $k = 46.8$ N/m. Interactions between liquid particles and between liquid and solid particles were modeled by a LJ pair potential, $\Phi_{LJ}(r) = 4\epsilon_{ij}[(\sigma_{ij}/r)^{12} - (\sigma_{ij}/r)^6]$, where i, j can be L for liquid particles or S for solid particles. The LJ interaction was truncated at a cut-off distance of $r_c = 3.5\sigma$ and quadratic functions were added so that the potential and interaction force smoothly vanished at r_c .⁵⁵ We used $\sigma_{LL} = 0.34$ nm, $\epsilon_{LL} = 121$ K k_B , $\sigma_{LS} = 0.345$ nm, and $\epsilon_{LS} = \alpha\epsilon_{LL}$, where the “wetting coefficient” α was varied between 0.120 and 0.359. The corresponding contact angle of droplets with these parameters was shown in our previous work.⁵⁶ The atomic masses were $m_L = 39.95$ u and $m_S = 195.1$ u. We used periodic boundary conditions along the x and y lateral directions, with a box size $L_x = L_y = 6.27$ nm. The total system height (walls included) along the z direction was varied between 4 and 12 nm, with a corresponding number of liquid particles varying between ~ 800 and 6400. We defined the liquid film height as $H_{liq} = z_{wall}^{top} - z_{wall}^{bottom}$, with z_{wall}^{top} and z_{wall}^{bottom} being the positions where the liquid density vanishes, which can be accurately identified due to the steep rise of the density at the interface, see Fig. 1. Accordingly, H_{liq} varied between 1 and 9 nm. The above definition of z_{wall} was also used as the origin of δ_{eff} described later in Eq. (20).

To compare the GK measurement and a reference NEMD measurement of the friction coefficient in the same system, we sheared the liquid in the x direction to extract the nonequilibrium response and we applied the GK formalism in the y direction. We checked on representative systems that independent EMD and NEMD simulations provided results consistent with the ones obtained using

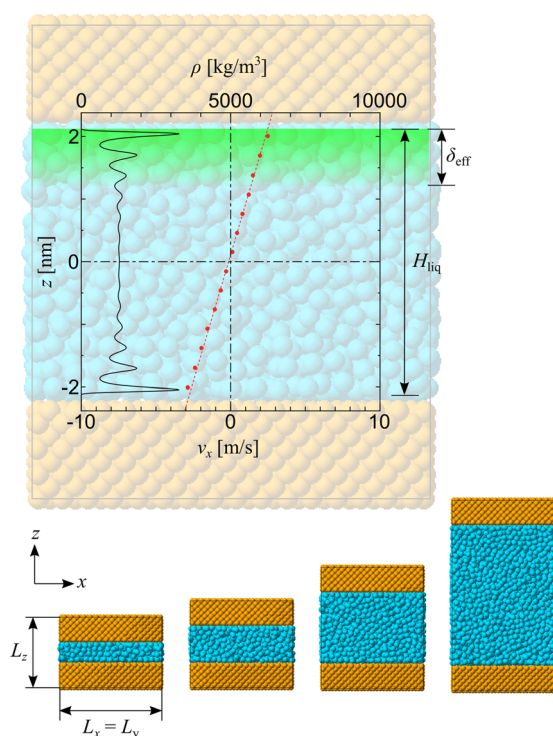


FIG. 1. Top: side view of a typical simulated system, superimposed with the corresponding density and velocity profiles. Bottom: side views of systems with different heights.

this approach. In practice, particles in the most external layer of the walls were fixed in the y direction, and we imposed a shear force per area $\tau_w = 0.2$ MPa by applying opposite forces $F_w = \pm \tau_w \times S$ in the x direction to the most external particles of the top/bottom wall, respectively. Particles in the second most external layer were

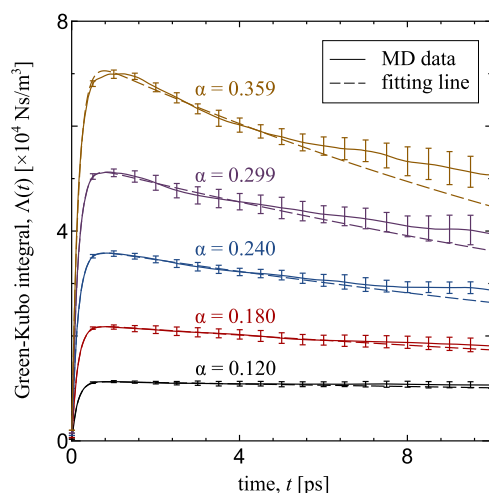


FIG. 2. Green-Kubo integrals $\Lambda(t)$ obtained for different wetting coefficients α . Full lines: MD data and dashed lines: fits with Eq. (13).

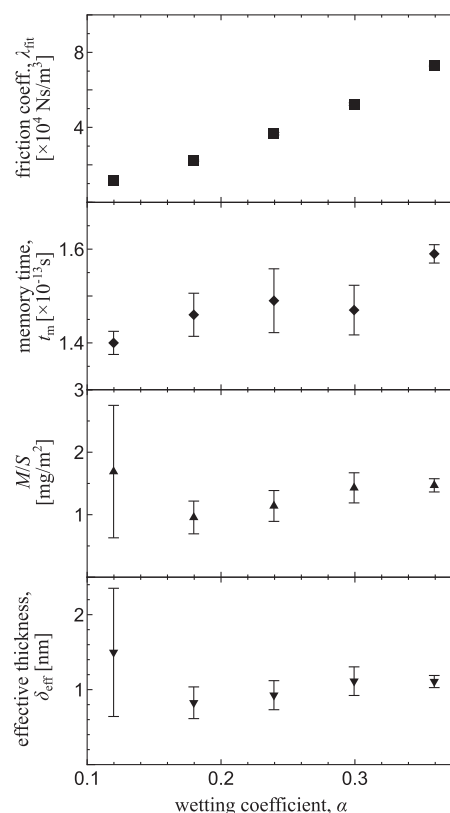


FIG. 3. Evolution of λ_{fit} , t_m , M/S , and the corresponding δ_{eff} with the wetting coefficient α . For λ_{fit} , the error bars are smaller than the symbols.

thermostatted at 100 K using a Langevin thermostat applied only in the z direction. We checked that the liquid temperature remained within 2 K of the set value. To set the pressure to 4 MPa, we first used the top wall as a piston, without shear; second, we applied shear, still using the top wall as a piston; and finally, we fixed the vertical wall position and continued shearing the system. We integrated the equations of motion using the velocity-Verlet algorithm, with a time step of 5 fs. The simulation time was 50 ns. Error bars in Figs. 2, 3, and 6 were obtained by separating the production run into five 10 ns chunks, measuring the quantities for each chunk, and estimating the statistical error within a 95% confidence interval from the five values.

IV. RESULTS AND DISCUSSION

We first computed the GK integrals $\Lambda(t)$ for different wetting coefficients α , see Fig. 2. For low α (nonwetting surfaces), friction is low so that the decay time t_d given by Eq. (12) is large and a plateau of the GK integral is observed at times intermediate between the memory kernel time t_m and the decay time t_d . However, as α increases, so does the friction coefficient. As a consequence, the GK integral goes to higher values, and the decay time decreases; for large α , t_d becomes comparable with t_m so that one cannot observe a plateau of the GK integral anymore. In that situation, the original BB formula

cannot be directly applied and we used our finite-size extension of the formula, Eq. (13), to fit the GK integrals. Since at long times the error on the GK integrals becomes large, the numerical data were fitted for times $t < 5$ ps. The model indeed reproduces well the MD data at short and intermediate times, see Fig. 2.

From the fit of the GK integrals, one can extract the values of the friction coefficient λ_{fit} , of the coarse-grained mass per unit surface M/S , and of the memory kernel relaxation time t_m . The evolution of these parameters with the wetting coefficient α is shown in Fig. 3. While the friction coefficient strongly depends on the wetting coefficient α , the memory kernel time t_m remains constant within the error bars, at a value of ~ 150 fs (except at the highest α where it is larger by $\lesssim 10\%$). This value is typical of viscoelastic relaxation in liquids. The effective mass of the coarse-grained system in the Langevin description increases slightly beyond the error bars with α , from ~ 1 to 1.5 mg/m². The fact that the effective mass does not depend much on α suggests that the description of the decay time as a function only of the liquid-solid friction coefficient and of a coarse-grained mass (enclosing effectively the liquid hydrodynamic modes), Eq. (12), is adequate in all systems considered. Note however that for the largest values of α , corresponding to the largest friction coefficients and smallest decay times t_d , a slower decay of the GK integral seems to appear at long times, which is not captured by Eq. (13). This slower time scale could be related to momentum diffusion through the liquid, which by construction the coarse-grained description cannot capture. We will come back to that point when discussing the dependency of the GK integral with the system height.

We then computed the effective thickness δ_{eff} of the coarse-grained system corresponding to the effective mass M/S , by integrating the liquid density profiles $\rho_{\text{liq}}(z)$ near the wall,

$$\frac{M}{S} = \int_{z_{\text{wall}}}^{z_{\text{wall}} + \delta_{\text{eff}}} \rho_{\text{liq}}(z) dz. \quad (20)$$

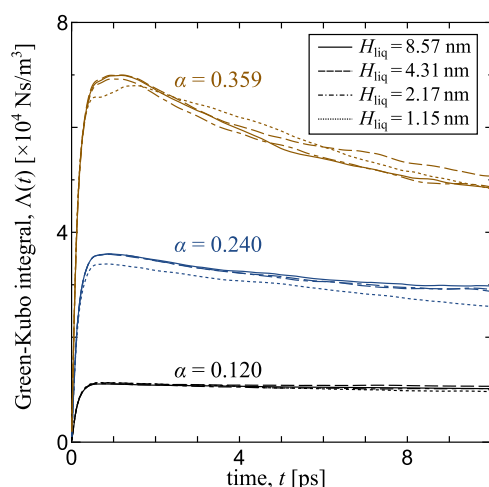


FIG. 4. Comparison of the GK integrals obtained for different wetting coefficients α and for different system heights H_{liq} . Since H_{liq} depends slightly on α for a given number of atoms, the H_{liq} values for systems with $\alpha = 0.240$ are shown in the figure.

In Fig. 3, one can observe that the increase of δ_{eff} with α is similar to that of M/S .

Interestingly, δ_{eff} is on the order of 2–3 molecular sizes, i.e., the coarse-grained system of interest in the Langevin equation involves only a thin region of liquid close to the interface. Accordingly, the GK integrals should not depend on the system height for heights larger than δ_{eff} .

We tested the influence of system height on the GK integral for different wetting coefficients α . Figure 4 shows that, as expected from the small effective thickness of liquid whose fluctuations control the fluctuations of friction force, the GK integrals obtained for different liquid heights H_{liq} above 2.17 nm overlap so that their fit provides the same values for λ_{fit} , M/S , and t_m . On the other hand, the GK integrals obtained for the smallest liquid height $H_{\text{liq}} = 1.15$ nm, which is comparable to δ_{eff} in Fig. 3, are significantly different from those for $H_{\text{liq}} \geq 2.17$ nm. This indicates that a certain liquid thickness is needed to apply the present method.

More quantitatively, Fig. 5 shows the dependence of the friction coefficient, memory time, effective mass, and corresponding thickness on the liquid height H_{liq} for systems with $\alpha = 0.240$. As suggested by the GK curves in Fig. 4, neither λ nor M/S depend on H_{liq} above a certain value so that the decay time $t_d = M/(\lambda S)$ is also independent of the liquid height. The independence of t_d on the system size seems to suggest that the GK integral $\Lambda(t)$ will always vanish

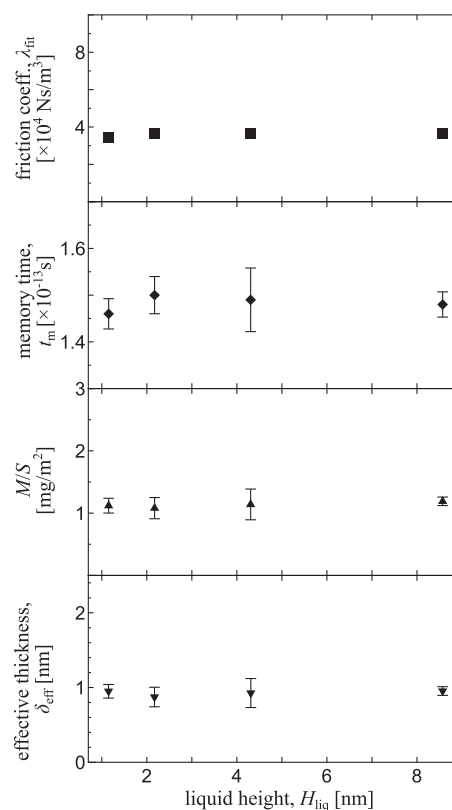


FIG. 5. Evolution of λ_{fit} , t_m , M/S , and the corresponding δ_{eff} with the liquid height H_{liq} for systems with $\alpha = 0.240$.

at infinite time regardless of the system size, and in particular at the thermodynamic limit. However, we have already mentioned that the coarse-grained description, while it worked very well to describe the GK integral at short and intermediate times, failed to describe a slower decay of the GK integral at long times. One can imagine two other characteristic time scales related to the momentum diffusion, i.e., $t_{\text{visc}}(\delta_{\text{eff}}) \sim \delta_{\text{eff}}^2/\nu$ and $t_{\text{visc}}(H_{\text{liq}}) \sim H_{\text{liq}}^2/\nu$, where ν is the kinematic viscosity of the liquid. Using the bulk value $\nu \approx 1.1 \times 10^{-7} \text{ m}^2/\text{s}$, the former is roughly estimated about 9 ps with $\delta_{\text{eff}} \sim 1 \text{ nm}$, and the latter is from 12 ps to 670 ps with H_{liq} for the present systems. These longer time scales should largely affect the asymptotic behavior. In particular, the second time scale diverges for infinite system height.

Finally, we compare the presented method to estimate the friction coefficient, λ_{fit} , with the reference NEMD measurement, and with the maximum of the GK integral, Λ_{max} . The NEMD friction coefficient was computed using Eq. (1), where we tested two definitions for the slip velocity: first, we measured the difference between the wall velocity and the liquid velocity at the position of the first adsorption layer z_1 , $v_s = |v_{\text{liquid}}(z_1) - v_{\text{wall}}|$; second, we computed the difference between the wall velocity and the extrapolated bulk liquid velocity profile at the position of the first adsorption layer, $v_s = |v_{\text{extrapolated}}(z_1) - v_{\text{wall}}|$. The NEMD friction coefficients obtained from these two definitions are denoted as $\lambda_{\text{NE,liq}}$ and $\lambda_{\text{NE,ext}}$, respectively.

Figure 6 compares the different measurements for varying the wetting coefficient. First, we note that the difference between λ_{fit} and Λ_{max} is less than 5%. Since in the systems considered, the time scale ratio $u = t_2/t_1$ was on the order of 1/100 or less, the relative error between Λ_{max} and λ_{fit} is consistent with the estimate provided in Sec. II. In practice, this means that, at least for the systems considered here, simply measuring the maximum of the GK integral provides a good estimate of the friction coefficient.

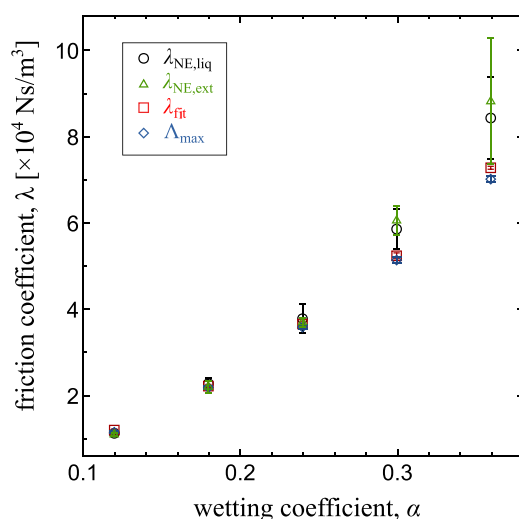


FIG. 6. Comparison between different measurements of the friction coefficient [NEMD measurements, $\lambda_{\text{NE,liq}}$ and $\lambda_{\text{NE,ext}}$, maximum of the GK integral, Λ_{max} , and value obtained from fitting with Eq. (13), λ_{fit} , see text for details] as a function of the wetting coefficient α .

We then turn to the NEMD measurements. One can notice that the error bars are much larger for the NEMD points than for the EMD points, even though the data were obtained for the same simulation time. This suggests that EMD provides a more efficient route to measure liquid-solid friction than NEMD. In addition, two different approaches to measure the slip velocity, i.e., based on the fluid velocity in the first adsorption layer, $\lambda_{\text{NE,liq}}$ or based on the extrapolated bulk velocity profile at the same position, $\lambda_{\text{NE,ext}}$, result in different values for the friction coefficient. The NEMD measurement will also depend on the position where the slip velocity is measured. While using the position of the first adsorption layer is common practice, this approach has no firm fundamental basis.

Overall, the NEMD estimate is therefore less accurate for a given simulation time and sensitive to the procedure used to determine the slip velocity. In contrast, fitting the GK integral provides an accurate and unambiguous value. Although the EMD and NEMD seem to deviate at large wetting coefficients α , the difference is within the error bars. Additionally, we would like to emphasize that for the largest values of α , the friction coefficient is very large and corresponds to very small slip lengths, $b \sim 1 \text{ nm}$. For such values of b , any uncertainty on the hydrodynamic wall position will result in a large error on the friction coefficient so that we suggest that EMD should here be thought as the reference measurement method and that the apparent discrepancy between EMD and NEMD highlights the difficulties of getting a proper NEMD estimate in the studied systems.

V. CONCLUSION

The BB formula, identifying the liquid-solid friction coefficient with the plateau value of a GK integral, poses some problems in finite-size simulations, where the GK integral vanishes at long times. This formula can be obtained from a Langevin description of a diffusing wall in contact with a semi-infinite liquid. Here, we derived the analytical expression of the GK integral for a finite-size liquid slab confined between immobile walls by applying the Langevin description to a coarse-grained system involving effectively a fraction of the confined liquid, assuming a simple Maxwell-type memory kernel relating the slip velocity and velocity of the coarse-grained system. Using this generic analytical framework, we showed that a common procedure of taking the maximum of the GK integral as the friction coefficient was reasonably accurate when the memory time and the decay time of the GK integral were well separated (e.g., a 4% error for a factor of 100 between the two times).

By fitting MD results to the derived expression, we could extract the friction coefficient, the memory time, the mass of the coarse-grained system, and the corresponding effective thickness of liquid whose fluctuations control the fluctuations of the friction force. We varied the wetting properties by tuning the liquid-solid interaction potential. The friction coefficient was strongly affected by wetting, while the memory time remained approximately constant, at a value consistent with viscoelastic relaxation. The effective thickness δ_{eff} of fluctuating liquid did not change much and was on the order of 2–3 molecular sizes. Accordingly, we checked that the measured friction coefficient was independent of the liquid film height H_{liq} when it remained large as compared to δ_{eff} . For a smaller system with $H_{\text{liq}} \sim \delta_{\text{eff}}$, the GK integrals changed. The estimate of δ_{eff} from the fit of the GK integral therefore provides a self-consistent criterion on

the minimal system height that needs to be used to characterize interfacial friction without confinement effects.

Finally, we compared EMD and NEMD measurements. For a given simulation time, the approach presented here provides a lower statistical error; additionally, in NEMD an ambiguity on the measured friction coefficient results from the difficulty of defining the slip velocity, but in the proposed method the slip velocity does not need to be defined. Overall, we suggest that the proposed approach is simple and accurate, and provides an efficient path to characterize liquid-solid friction in MD simulations.

ACKNOWLEDGMENTS

Y.Y. and T.O. were supported by JSPS KAKENHI Grant Nos. JP18K03978 and JP18K03929, Japan, respectively. Y.Y. was also supported by JST CREST Grant No. JPMJCR18I1, Japan. This work was supported by the ANR, Project No. ANR-16-CE06-0004-01 NEC-tAR. L.J. was supported by the Institut Universitaire de France. L.J. benefited from a JSPS international fellowship for research in Japan.

APPENDIX: COMPLETE DERIVATION

Here is the derivation of Bocquet-Barrat formula

$$\lambda = \frac{1}{Sk_B T} \int_0^\infty \langle F_w(0)F_w(t) \rangle dt. \quad (\text{A1})$$

We start from the generalized Langevin equation (GLE)⁵¹

$$M \frac{dU}{dt} = -S \int_{-\infty}^t \lambda'(t-t')U(t')dt' + R(t), \quad (\text{A2})$$

where M and U are the mass and velocity of the coarse-grained system of interest, respectively, while S , λ' , and $R(t)$ denote the surface area, retarded effect of the friction, and random force, respectively. The macroscopic friction coefficient λ is related to λ' by⁴⁵

$$\lambda = \int_0^\infty \lambda'(t)dt. \quad (\text{A3})$$

By substituting $\lambda'(t) = \lambda\xi(t)$ with a memory kernel ξ , which satisfies

$$\int_0^\infty \xi(t)dt = 1, \quad (\text{A4})$$

it follows for Eq. (A2) that

$$M \frac{dU}{dt} = -\lambda S \int_{-\infty}^t \xi(t-t')U(t')dt' + R(t). \quad (\text{A5})$$

Note that in the case the wall is mobile as in the theoretical derivation of Bocquet and Barrat,²¹ the mass and velocity are replaced by wall mass and velocity M_w and U_w , respectively, and the slip velocity v_s and U_w are related by

$$v_s(t) = \int_{-\infty}^t \xi(t-t')U_w(t')dt'. \quad (\text{A6})$$

A Green-Kubo relation is derived from the GLE, Eq. (A5), through the Laplace transform. By multiplying $U(0)$ to both sides of Eq. (A5) and by taking the ensemble average, it follows that

$$M \left\langle U(0) \frac{dU(t)}{dt} \right\rangle = -\lambda S \int_{-\infty}^t \xi(t-t') \langle U(0)U(t') \rangle dt' + \langle U(0)R(t) \rangle. \quad (\text{A7})$$

Denoting $C_U(t) \equiv \langle U(0)U(t) \rangle$ the equilibrium autocorrelation function of U and assuming $\langle U(0)R(t) \rangle = 0$ for $t \geq 0$, Eq. (A7) is rewritten as

$$\frac{dC_U(t)}{dt} = -t_d^{-1} \int_0^t \xi(t-t')C_U(t')dt', \quad (\text{A8})$$

where the lower limit of the integral is changed from $-\infty$ to 0 so that $C_U(t)$ satisfies the stationarity condition,^{51,52} i.e., $C_U(t)$ is an even function. In addition, the decay time scale t_d given by

$$t_d \equiv \frac{M}{\lambda S} \quad (\text{A9})$$

is introduced. Let the Laplace transform $\mathcal{L}(f) \equiv \tilde{f}(s)$ of a function $f(t)$ be denoted by

$$\mathcal{L}(f) \equiv \tilde{f}(s) = \int_0^\infty f(t)e^{-st}dt. \quad (\text{A10})$$

Then, the Laplace transform of Eq. (A8) is written as

$$s\tilde{C}_U(s) - C_U(0) = -t_d^{-1}\tilde{\xi}(s)\tilde{C}_U(s). \quad (\text{A11})$$

By using the energy equipartition

$$C_U(0) = \langle U^2 \rangle = \frac{k_B T}{M} \quad (\text{A12})$$

for the second term of the LHS of Eq. (A11), it follows that

$$\tilde{C}_U(s) = \frac{k_B T}{M} \frac{1}{s + t_d^{-1}\tilde{\xi}(s)}. \quad (\text{A13})$$

On the other hand, the force $F_w(t)$ exerted on the coarse-grained system of interest is given by

$$F_w(t) = M \frac{dU}{dt}. \quad (\text{A14})$$

Then, the autocorrelation function $C_F(t) = \langle F_w(0)F_w(t) \rangle$ of the force F_w , satisfies the following relation:⁵⁰

$$C_F(t) = -M^2 \frac{d^2 C_U(t)}{dt^2}. \quad (\text{A15})$$

By using this, we examine the function form of the integrated force autocorrelation function $\Lambda(t)$ given by

$$\Lambda(t) \equiv \frac{1}{Sk_B T} \int_0^t C_F(t')dt' = -\frac{M^2}{Sk_B T} \left(\frac{dC_U(t)}{dt} - \frac{dC_U(t)}{dt} \Big|_{t=0} \right), \quad (\text{A16})$$

where $\frac{dC_U(t)}{dt} \Big|_{t=0} = 0$ considering that $C_U(t)$ is an even function due to the stationarity condition.⁵¹⁻⁵⁴ Note that

$$\left. \frac{dC_U(t)}{dt} \right|_{t=0} \equiv \frac{1}{2} \left(\left. \frac{dC_U(t)}{dt} \right|_{t=0^+} + \left. \frac{dC_U(t)}{dt} \right|_{t=0^-} \right) = 0 \quad (\text{A17})$$

should be applied in the case the memory kernel $\xi(t)$ is equal to the Dirac delta function, i.e., Eq. (3) is a simple Langevin equation, where $\frac{dC_U(t)}{dt}$ has a discontinuous derivative at $t = 0$, see Refs. 21 and 54. Bocquet and Barrat²¹ technically dealt with this by setting the lower limit of integration in Eq. (A10) as 0^- instead of 0. The Laplace transform of the above equation is

$$\tilde{\Lambda}(s) = -\frac{M^2}{S k_B T} (s \tilde{C}_U(s) - C_U(0)). \quad (\text{A18})$$

By inserting Eqs. (A12) and (A13) into Eq. (A18), it follows that

$$\tilde{\Lambda}(s) = \frac{M}{S} \frac{t_d^{-1} \tilde{\xi}(s)}{s + t_d^{-1} \tilde{\xi}(s)} = \frac{\lambda \tilde{\xi}(s)}{s + t_d^{-1} \tilde{\xi}(s)}. \quad (\text{A19})$$

We now assume the following Maxwell-type memory kernel:⁵⁰

$$\xi(t) = t_m^{-1} e^{-\frac{t}{t_m}} \quad (t \geq 0). \quad (\text{A20})$$

The Laplace transform of this memory kernel is

$$\tilde{\xi}(s) = \frac{t_m^{-1}}{s + t_m^{-1}}. \quad (\text{A21})$$

By inserting Eq. (A21) into Eq. (A19), it follows that

$$\tilde{\Lambda}(s) = \frac{\lambda}{t_m (s^2 + t_m^{-1} s + t_m^{-1} t_d^{-1})}. \quad (\text{A22})$$

We factorize the denominator of Eq. (A22) as

$$s^2 + \frac{1}{t_m} s + \frac{1}{t_m t_d} = \left(s + \frac{1}{t_1}\right) \left(s + \frac{1}{t_2}\right) \quad (\text{A23})$$

with

$$\frac{1}{t_1} = \frac{1}{2t_m} \left(1 - \sqrt{1 - \frac{4t_m}{t_d}}\right), \quad (\text{A24})$$

$$\frac{1}{t_2} = \frac{1}{2t_m} \left(1 + \sqrt{1 - \frac{4t_m}{t_d}}\right), \quad (\text{A25})$$

which are real as long as $t_d > 4t_m$. Then, it follows from Eq. (A22) that

$$\tilde{\Lambda}(s) = \frac{\lambda}{t_m \left(s + \frac{1}{t_1}\right) \left(s + \frac{1}{t_2}\right)} = \lambda_0 \left(\frac{1}{s + \frac{1}{t_1}} - \frac{1}{s + \frac{1}{t_2}} \right)$$

with

$$\lambda_0 \equiv \frac{\lambda}{t_m \left(\frac{1}{t_2} - \frac{1}{t_1}\right)} = \frac{\lambda}{\sqrt{1 - \frac{4t_m}{t_d}}}. \quad (\text{A26})$$

With these three parameters t_1 , t_2 , and λ_0 , we obtain an analytical solution of $\Lambda(t)$ as

$$\Lambda(t) = \lambda_0 \left(e^{-\frac{t}{t_1}} - e^{-\frac{t}{t_2}} \right). \quad (\text{A27})$$

In the limit of $t_d \gg t_m$,

$$\frac{1}{t_1} \approx \frac{1}{t_d} \left(1 - \frac{t_m}{t_d}\right), \quad \frac{1}{t_2} \approx \frac{1}{t_m} \left(1 - \frac{t_m}{t_d}\right), \quad \lambda_0 \approx \lambda \left(1 + \frac{2t_m}{t_d}\right). \quad (\text{A28})$$

This gives two behaviors: for $t_d \rightarrow \infty$,

$$\Lambda(t) \approx \lambda \left(1 - e^{-\frac{t}{t_m}}\right), \quad (\text{A29})$$

i.e., the GK integral reaches a plateau value equal to the friction coefficient, which corresponds to the original BB result. On the other hand, Eq. (A27) for finite t_d with $t_m \rightarrow 0$ results in

$$\Lambda(t) \approx \lambda e^{-\frac{t}{t_d}}, \quad (\text{A30})$$

which is expected in a finite system.⁴⁵

REFERENCES

1. Bocquet and E. Charlaix, "Nanofluidics, from bulk to interfaces," *Chem. Soc. Rev.* **39**, 1073–1095 (2010).
2. L. Bocquet and P. Tabeling, "Physics and technological aspects of nanofluidics," *Lab Chip* **14**, 3143–3158 (2014).
3. A. Siria, P. Poncharal, A.-L. Biance, R. Fulcrand, X. Blase, S. T. Purcell, and L. Bocquet, "Giant osmotic energy conversion measured in a single transmembrane boron nitride nanotube," *Nature* **494**, 455–458 (2013).
4. J. Feng, M. Graf, K. Liu, D. Ovchinnikov, D. Dumcenco, M. Heiranian, V. Nandigana, N. R. Aluru, A. Kis, and A. Radenovic, "Single-layer MoS₂ nanopores as nanopower generators," *Nature* **536**, 197–200 (2016).
5. A. Siria, M.-L. Bocquet, and L. Bocquet, "New avenues for the large-scale harvesting of blue energy," *Nat. Rev. Chem.* **1**, 0091 (2017).
6. S. J. Kim, S. H. Ko, K. H. Kang, and J. Han, "Direct seawater desalination by ion concentration polarization," *Nat. Nanotechnol.* **5**, 297–301 (2010).
7. D. Cohen-Tanugi and J. C. Grossman, "Water desalination across nanoporous graphene," *Nano Lett.* **12**, 3602–3608 (2012).
8. A. Striolo, A. Michaelides, and L. Joly, "The carbon-water interface: Modeling challenges and opportunities for the water-energy nexus," *Ann. Rev. Chem. Biomol.* **7**, 533–556 (2016).
9. C. Neto, D. R. Evans, E. Bonaccorso, H.-J. Butt, and V. S. J. Craig, "Boundary slip in Newtonian liquids: A review of experimental studies," *Rep. Prog. Phys.* **68**, 2859–2897 (2005).
10. L. Bocquet and J.-L. Barrat, "Flow boundary conditions from nano- to micro-scales," *Soft Matter* **3**, 685–693 (2007).
11. C. Navier, "Mémoire sur les lois du mouvement des fluides," *Mem. Acad. Sci. Inst. Fr.* **6**, 389 (1823).
12. B. Cross, C. Barraud, C. Picard, L. Léger, F. Restagno, and E. Charlaix, "Wall slip of complex fluids: Interfacial friction versus slip length," *Phys. Rev. Fluids* **3**, 062001 (2018).
13. L. Bocquet and J. L. Barrat, "Hydrodynamic boundary conditions, correlation functions, and Kubo relations for confined fluids," *Phys. Rev. E* **49**, 3079–3092 (1994).
14. C. J. Mundy, S. Balasubramanian, and M. L. Klein, "Hydrodynamic boundary conditions for confined fluids via a nonequilibrium molecular dynamics simulation," *J. Chem. Phys.* **105**, 3211–3214 (1996).
15. C. J. Mundy, S. Balasubramanian, and M. L. Klein, "Computation of the hydrodynamic boundary parameters of a confined fluid via non-equilibrium molecular dynamics," *Physica A* **240**, 305–314 (1997).
16. J. Delhomme and P. T. Cummings, "Simulation of friction in nanoconfined fluids for an arbitrarily low shear rate," *Phys. Rev. B* **72**, 172201 (2005).
17. J. Petrávic and P. Harrowell, "On the equilibrium calculation of the friction coefficient for liquid slip against a wall," *J. Chem. Phys.* **127**, 174706 (2007).
18. V. P. Sokhan and N. Quirke, "Slip coefficient in nanoscale pore flow," *Phys. Rev. E* **78**, 015301 (2008).

- ¹⁹J. S. Hansen, B. D. Todd, and P. J. Daivis, "Prediction of fluid velocity slip at solid surfaces," *Phys. Rev. E* **84**, 016313 (2011).
- ²⁰S. K. Kannam, B. D. Todd, J. S. Hansen, and P. J. Daivis, "Slip length of water on graphene: Limitations of non-equilibrium molecular dynamics simulations," *J. Chem. Phys.* **136**, 024705 (2012).
- ²¹L. Bocquet and J.-L. Barrat, "On the Green-Kubo relationship for the liquid-solid friction coefficient," *J. Chem. Phys.* **139**, 044704 (2013).
- ²²K. Huang and I. Szlufarska, "Green-Kubo relation for friction at liquid-solid interfaces," *Phys. Rev. E* **89**, 032119 (2014).
- ²³S. Chen, H. Wang, T. Qian, and P. Sheng, "Determining hydrodynamic boundary conditions from equilibrium fluctuations," *Phys. Rev. E* **92**, 043007 (2015).
- ²⁴B. Ramos-Alvarado, S. Kumar, and G. P. Peterson, "Hydrodynamic slip length as a surface property," *Phys. Rev. E* **93**, 023101 (2016).
- ²⁵A. Sam, R. Hartkamp, S. K. Kannam, and S. P. Sathian, "Prediction of fluid slip in cylindrical nanopores using equilibrium molecular simulations," *Nanotechnology* **29**, 485404 (2018).
- ²⁶P. A. Thompson and M. O. Robbins, "Shear flow near solids: Epitaxial order and flow boundary conditions," *Phys. Rev. A* **41**, 6830–6837 (1990).
- ²⁷P. A. Thompson and S. M. Troian, "A general boundary condition for liquid flow at solid surfaces," *Nature* **389**, 360–362 (1997).
- ²⁸J. Barrat and L. Bocquet, "Influence of wetting properties on hydrodynamic boundary conditions at a fluid/solid interface," *Faraday Discuss.* **112**, 119–127 (1999).
- ²⁹M. Cieplak, J. Koplik, and J. R. Banavar, "Boundary conditions at a fluid-solid interface," *Phys. Rev. Lett.* **86**, 803–806 (2001).
- ³⁰K. Falk, F. Sedlmeier, L. Joly, R. R. Netz, and L. Bocquet, "Molecular origin of fast water transport in carbon nanotube membranes: Superlubricity versus curvature dependent friction," *Nano Lett.* **10**, 4067–4073 (2010).
- ³¹S. K. Kannam, B. D. Todd, J. S. Hansen, and P. J. Daivis, "How fast does water flow in carbon nanotubes?," *J. Chem. Phys.* **138**, 094701 (2013).
- ³²S. K. Bhatia and D. Nicholson, "Friction between solids and adsorbed fluids is spatially distributed at the nanoscale," *Langmuir* **29**, 14519–14526 (2013).
- ³³G. Tocci, L. Joly, and A. Michaelides, "Friction of water on graphene and hexagonal boron nitride from *ab initio* methods: Very different slippage despite very similar interface structures," *Nano Lett.* **14**, 6872–6877 (2014).
- ³⁴L. Guo, S. Chen, and M. O. Robbins, "Slip boundary conditions over curved surfaces," *Phys. Rev. E* **93**, 013105 (2016).
- ³⁵S. Nakaoka, Y. Yamaguchi, T. Omori, and L. Joly, "Molecular dynamics analysis of the friction between a water-methanol liquid mixture and a non-polar solid crystal surface," *J. Chem. Phys.* **146**, 174702 (2017).
- ³⁶S. Bernardi, B. D. Todd, and D. J. Searles, "Thermostating highly confined fluids," *J. Chem. Phys.* **132**, 244706 (2010).
- ³⁷M. Thomas and B. Corry, "Thermostat choice significantly influences water flow rates in molecular dynamics studies of carbon nanotubes," *Microfluid. Nanofluid.* **18**, 41–47 (2015).
- ³⁸A. Sam, S. K. Kannam, R. Hartkamp, and S. P. Sathian, "Water flow in carbon nanotubes: The effect of tube flexibility and thermostat," *J. Chem. Phys.* **146**, 234701 (2017).
- ³⁹P. Español and I. Zúñiga, "Force autocorrelation function in Brownian motion theory," *J. Chem. Phys.* **98**, 574–580 (1993).
- ⁴⁰L. Bocquet, J.-P. Hansen, and J. Piasecki, "Friction tensor for a pair of Brownian particles: Spurious finite-size effects and molecular dynamics estimates," *J. Stat. Phys.* **89**, 321–346 (1997).
- ⁴¹P. Español, J. A. de la Torre, and D. Duque-Zumajo, "Solution to the plateau problem in the Green-Kubo formula," *Phys. Rev. E* **99**, 022126 (2019).
- ⁴²S. Merabia and K. Termentzidis, "Thermal conductance at the interface between crystals using equilibrium and nonequilibrium molecular dynamics," *Phys. Rev. B* **86**, 094303 (2012).
- ⁴³A. Lagarkov and V. Sergeev, "Molecular dynamics method in statistical physics," *Usp. Fiz. Nauk* **125**, 409–448 (1978).
- ⁴⁴J. J. Brey and J. G. Ordóñez, "Computer studies of Brownian motion in a Lennard-Jones fluid: The Stokes law," *J. Chem. Phys.* **76**, 3260–3263 (1982).
- ⁴⁵J.-L. Barrat and F. Chiaruttini, "Kapitza resistance at the liquid–Solid interface," *Mol. Phys.* **101**, 1605–1610 (2003).
- ⁴⁶L. Joly, G. Tocci, S. Merabia, and A. Michaelides, "Strong coupling between nanofluidic transport and interfacial chemistry: How defect reactivity controls liquid–solid friction through hydrogen bonding," *J. Phys. Chem. Lett.* **7**, 1381–1386 (2016).
- ⁴⁷S. Nakaoka, Y. Yamaguchi, T. Omori, and L. Joly, "Extraction of the solid-liquid friction coefficient between a water-methanol liquid mixture and a non-polar solid crystal surface by Green-Kubo equations," *Mech. Eng. Lett.* **3**, 17–00422 (2017).
- ⁴⁸H. Nakano and S. Sasa, "Statistical mechanical expressions of slip length," *J. Stat. Phys.* **176**, 312–357 (2019).
- ⁴⁹D. Camargo, J. A. de la Torre, R. Delgado-Buscalioni, F. Chejne, and P. Español, "Boundary conditions derived from a microscopic theory of hydrodynamics near solids," *J. Chem. Phys.* **150**, 144104 (2019).
- ⁵⁰D. J. Evans and G. Morriss, *Statistical Mechanics of Nonequilibrium Liquids*, 2nd ed. (Cambridge University Press, 2008).
- ⁵¹R. Kubo, "The fluctuation-dissipation theorem," *Rep. Prog. Phys.* **29**, 255 (1966).
- ⁵²L. D. Landau and E. M. Lifshitz, *Statistical Physics*, 2nd ed. (Pergamon Press, 1969), p. 373.
- ⁵³B. J. Berne and R. Pecora, *Dynamic Light Scattering: With Applications to Chemistry, Biology, and Physics* (Dover Publications, 2000), p. 290.
- ⁵⁴J.-P. Hansen and I. R. McDonald, *Theory of Simple Liquids with Applications to Soft Matter*, 4th ed. (Academic Press, 2013), p. 283.
- ⁵⁵S. Nishida, D. Surblys, Y. Yamaguchi, K. Kuroda, M. Kagawa, T. Nakajima, and H. Fujimura, "Molecular dynamics analysis of multiphase interfaces based on *in situ* extraction of the pressure distribution of a liquid droplet on a solid surface," *J. Chem. Phys.* **140**, 074707 (2014).
- ⁵⁶Y. Yamaguchi, H. Kusudo, D. Surblys, T. Omori, and G. Kikugawa, "Interpretation of Young's equation for a liquid droplet on a flat and smooth solid surface: Mechanical and thermodynamic routes with a simple Lennard-Jones liquid," *J. Chem. Phys.* **150**, 044701 (2019).